POLITECNICO DI TORINO
Repository ISTITUZIONALE

Piezo- and Photocatalytic Activity of Ferroelectric ZnO:Sb Thin Films for the Efficient Degradation of Rhodamine- dye Pollutant

(Article begins on next page)

20 March 2024

Piezo- and photocatalytic activity of ferroelectric ZnO:Sb thin films for the efficient degradation of Rhodamine-β dye pollutant

Marco Laurenti[1], Nadia Garino[1,2], Giancarlo Canavese[1], Simelys Hernandéz[1,2], and Valentina Cauda[1] *

[1]Department of Applied Science and Technology, Politecnico di Torino, C.so Duca degli Abruzzi 24, 10129 Turin (Italy)

[2]Center for Sustainable Future Technologies @Polito, Istituto Italiano di Tecnologia, Via Livorno, 60, 10144 Turin, Italy

ABSTRACT The discovery of novel catalytic materials showing unprecedented properties and improved functionalities represents a major challenge to design advanced oxidation

processes for wastewater purification. In this work, antimony (Sb) doping is proposed as

a powerful approach for enhancing the photo- and piezocatalytic performances of

piezoelectric zinc oxide (ZnO) thin films. To investigate the role played by the dopant, the

degradation of Rhodamine-β (Rh-β), a dye pollutant widely present in natural water

sources, is studied when the catalyst is irradiated by ultraviolet (UV) light or ultrasound

(US) waves. Depending on the doping level, the structural, optical and ferroelectric

properties of the catalyst can be properly set to maximize the dye degradation efficiency.

Independently of the irradiation source, the fastest and complete dye degradation is

observed in presence of the doped catalyst and for an optimal amount of the inserted

dopant. Among ZnO:Sb samples, the most doped one (5 at.%) shows improved UV light

absorption and photocatalytic properties. Conversely, the piezocatalytic efficiency is

maximized using the lowest Sb amount (1 at.%). The superior ferroelectric polarization

observed in this case highly favors the adsorption of electrically-charged species, in

particular of the dye in the protonated form (Rh-β$^+$) and of OH$^-$, to the catalyst surface and

the production of hydroxyl radicals responsible for dye degradation.

1
2
3
4
5
6
7
8
9
10
11
12
13
14
15
16
17
18
19
20
21
22
23
24
25
26
27
28
29
30
31
32
33
34
35
36
37
38
39
40
41
42
43
44
45
46
47
48
49
50
51
52
53
54
55
56
57
58
59
60

1. Introduction

In the recent years, the problem of wastewater treatment is capturing considerable

attention because of the alarming decrease in natural resources of clean water.[1] Among

water pollutants, Rhodamine B (Rh-β) is by far one of the mostly abundant and its

presence in the environment has to be completely avoided because of its carcinogenic

and mutagenic effects on living species.[2]

The conventional treatments to remove pollutants from water are based on either

physical, chemical or biological processes. Some examples include chemical

precipitation, ion exchange, adsorption and membrane filtration.[3] Despite their

widespread use, these methods show several drawbacks such as long processing times

and reduced removal efficiencies. In order to overcome the abovementioned limitations,

advanced oxidation processes (AOPs) have received a lot of attention thanks to their

superior performances in terms of removal of pollutants.[3] AOPs are designed to degrade

organic compounds by oxidation through reaction with reactive oxygen species (ROS),

such as hydroxyl radical, superoxide radical anion, hydrogen peroxide and singlet

oxygen. Among AOPs, photocatalysis[4] and piezocatalysis[5] are the highly promising and

investigated approaches, and the discovery of novel catalyst materials sensitive to light and/or mechanical stimulation represents a major challenge to design AOPs for wastewater purification.

To this purpose, the use of semiconductor materials showing light absorption properties, piezoelectricity and ferroelectricity is emerging as strategy to prepare catalysts with improved functionalities.[6] In particular, the co-presence of photocatalytic properties and piezoelectricity would allow the use of light irradiation (ultraviolet, visible light, etc..) and mechanical stimulation (ultrasound, US) to induce a superior electron transfer between the catalyst and the wet chemical environment, increasing the number of redox electrochemical reactions and the generation of ROS responsible for dye degradation. At the same time, the presence of a ferroelectric polarization within the catalyst is expected to further improve the corresponding degradation efficiency thanks to a considerable reduction in the recombination rate of free carriers that generally limit the performances of the catalyst itself.

The piezocatalytic behavior of conventional piezoelectric materials has been recently investigated. Wu et al. successfully demonstrated the piezocatalytic activity of barium

titanate (BT) nanopowders and nanowires by considering the degradation of methyl

orange dye during ultrasonic vibration.[7] The observed piezocatalytic process was

explained according to the charge transfer model between the piezocatalyst and the dye

solution, and this was further corroborated by finite element method simulation. The large

piezoelectric potential of the considered BT nanostructures induced a greater shift of

conduction band and valance band. This resulted in an easier and faster migration of

electrons and holes during the reaction with dissolved oxygen and hydroxyls, promoting

the formation of singlet oxygen and hydroxyl radicals, and dye degradation. Other organic

dye pollutants have been degraded under ultrasonic vibrations using BT nanocrystals,[8]

micro-dendrites[9] and coral branches[10] as well, also with the aid of Fenton process in the

so-called "piezo-Fenton process".[10] Similarly, the piezocatalytic behavior of other

nanomaterials has been explored such as PZT fibers[11] and nanoparticles,[12] and $BiFeO_3$

nanosheets and nanowires.[13]

Despite the promising results, BT and PZT are non-biodegradable materials with limited

light absorption properties in their pure form. On the contrary, zinc oxide (ZnO) is a

generally-recognized-as-safe (GRAS) metal oxide semiconductor characterized by a

wide-band gap energy (3.37 eV) and strong absorption properties in the ultraviolet (UV)

light region.[14] Furthermore, ZnO is a piezoelectric semiconductor with a spontaneous

electrical polarization along the c-axis direction of the thermodynamically-stable wurtzite

crystalline phase.[15] ZnO is considered a low-cost material and it can exist in a huge

amount of morphologies and shapes.[16] High-surface-area ZnO micro- and nanostructures

can be easily prepared by following a variety of dry and wet chemical synthesis methods,

like sol-gel[17] and hydrothermal techniques[18] but also vapor phase deposition methods.[19]

Due to its semiconducting nature and light absorption properties, ZnO micro- and

nanostructures have been widely investigated for the photocatalytic degradation of

several dye pollutants such as Methylene Blue,[20] Rh-β[21] and Methyl Orange.[22] In each

case, the good catalytic activity of the considered ZnO morphologies, i.e., nanoparticles,

nanowires and microparticles,[21] has been successfully demonstrated and it has

confirmed the potential use of semiconductor ZnO-based catalysts for the successful

photodegradation of organic dyes. Independently of the morphology, the degradation

mechanism is explained in terms of UV photons absorption and the resulting generation

of free electron and hole pairs within the ZnO catalyst.[23] The electrons transfer between

the outermost surface of the ZnO catalyst and the surrounding environment leads to the

generation of reactive oxygen species (ROS), which induce dye breakage and

degradation. A similar behavior has been supposed to occur also during US irradiation of

ZnO nanowires for degrading methylene blue (MB), even combined with UV light

irradiation.[24] In this situation, a piezo-photocatalytic mechanism has been pointed out

thanks to the co-presence of UV light absorption and piezoelectric activity. This synergetic

effect resulted in a higher degradation efficiency.

On the other hand, ZnO-based materials suffer from a major drawback deriving from

the intrinsic n-type semiconducting behavior. This aspect limits the corresponding

catalytic efficiency since photo-generated carriers, which are at the base of

semiconductor-driven catalytic processes, can easily recombine together, thereby

affecting the final performances of the catalyst.[25] To this purpose, ZnO doping represents

a promising approach for tuning the corresponding electrical and optical properties.

Actually, the absorption range can be extended up to visible light[26] and the electrical

conduction behavior can be properly modulated as well, reducing the recombination

phenomena and enhancing the catalytic behavior.[25] Moreover, by properly selecting the

doping element, the electrical and piezoelectric properties of ZnO can be further improved

and combined together with unprecedented ferroelectric behavior,[27-29] resulting into new

generation materials with superior catalytic properties.[30-32]

In this work, antimony (Sb) is proposed as doping agent to improve the photo- and

piezocatalytic performances of piezoelectric zinc oxide (ZnO) films. To investigate the role

played by the dopant, the degradation of Rh-β is studied when the catalyst is irradiated

by UV light or ultrasound (US) waves. Independently of the irradiation source, the

complete degradation of the dye is achieved only in presence of the doped ZnO:Sb films.

Depending on the doping level, the structural, optical and ferroelectric properties of the

catalyst can be properly set to maximize the corresponding photo- and piezodegradation

efficiencies. Among ZnO:Sb samples, the mostly doped one (5 at.%) shows the highest

band-gap energy reduction and improved photocatalytic properties. Conversely, the

piezocatalytic efficiency is maximized using the lowest Sb amount (1 at.%). The superior

permanent ferroelectric polarization observed in the latter case is expected to limit free

carriers recombination, highly favors the adsorption of Rh-β^+ and OH^- electrically-charged

species to the catalyst surface and promotes a higher production of hydroxyl radicals responsible for dye degradation.

2. Results and Discussion

2.1. Physical and chemical properties of ZnO and ZnO:Sb thin films

The morphology of ZnO and ZnO:Sb thin films was investigated by means of field emission scanning electron microscopy (FESEM), as shown in Figure 1. The pristine ZnO thin film is obtained from sputtered Zn layers converted into ZnO by a thermal oxidation process. The as-prepared ZnO film (Figure 1a) is made of elongated and branched nanocrystals, forming a spongy-like nanoporous network. The existence of this peculiar morphology was previously reported by some of us,[33, 34] and its formation was explained by the structure zone model for thin-film growth and its extensions.[35] According to these models, this spongy-like nanostructure can be achieved by a proper combination of two process parameters; the melting temperature of the source material (in our case, a metallic Zn target) and the substrate temperature. In this work, this condition is achieved

by coupling the relatively low melting temperature of Zn source (690 K) and a local

temperature increase due to the impinging of sputtered particles on the substrate surface.

Regardless of the doping process, Figure 1 also highlights that no significant differences

are present among all the samples. Despite a slight increase of the crystal size for the

doped samples, both the pristine and doped ZnO thin films exhibit a similar morphology,

featuring a high-surface area porous framework made of highly-interconnected

nanocrystals.[34,37]

The presence of Sb in the doped samples is confirmed by elemental chemical analysis

obtained by energy dispersive X-ray spectroscopy (EDS). The corresponding spectra are

reported in Figure 2 and clearly show an increase in the amount of dopant for longer

impregnation times adopted in the synthetic procedure; it changes from 1 at.% to a

maximum amount of 5 at.% for the lowest (1 h) and highest time of impregnation (6 h),

respectively. High-resolution (HR) XPS measurements were also carried out in our

previous work,[28] revealing that Sb oxidation state in the ZnO:Sb doped samples is

influenced by the doping concentration (i.e., impregnation time). In particular, Sb ions are

involved in three different oxidation states: the main ones are Sb^{3+} and Sb^{5+} species while

a small Sb^0 fraction is detected as well. Sb^{3+} is the dominant one for doping levels up to

2 at.%. By increasing the doping amount, Sb^{5+} species become dominant together with

the a Sb^0 small contribution.
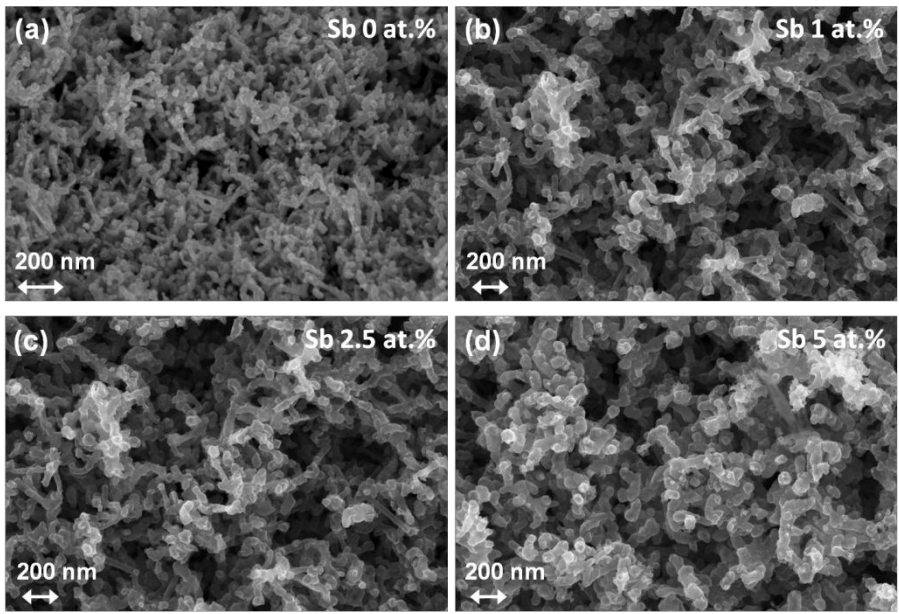
Figure 1. FESEM images of (a) pristine ZnO and (b-d) doped ZnO:Sb thin films

incorporating different amounts of Sb.

Element	Atomic %
C K	7.44
O K	51.10
Al K	0.17
Si K	0.11
Zn L	40.16
Sb L	1.02
Totals	100

Element	Atomic %
C K	6.75
O K	53.07
Al K	0.19
Si K	0.14
Zn L	37.37
Sb L	2.48
Totals	100

Element	Atomic %
C K	6.72
O K	55.82
Al K	0.22
Si K	0.19
Zn L	32.01
Sb L	5.04
Totals	100
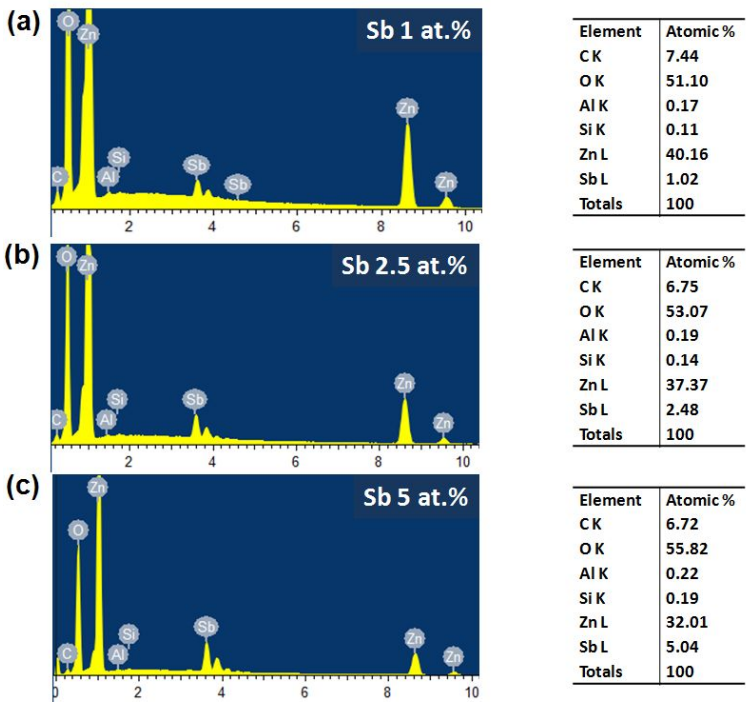
Figure 2. Energy Dispersive X-ray spectra and semi-quantitative analysis obtained for

ZnO:Sb thin films prepared with different doping levels: (a) Sb 1 at.%; (b) Sb 2.5 at.%; (c)

Sb 5 at.%.
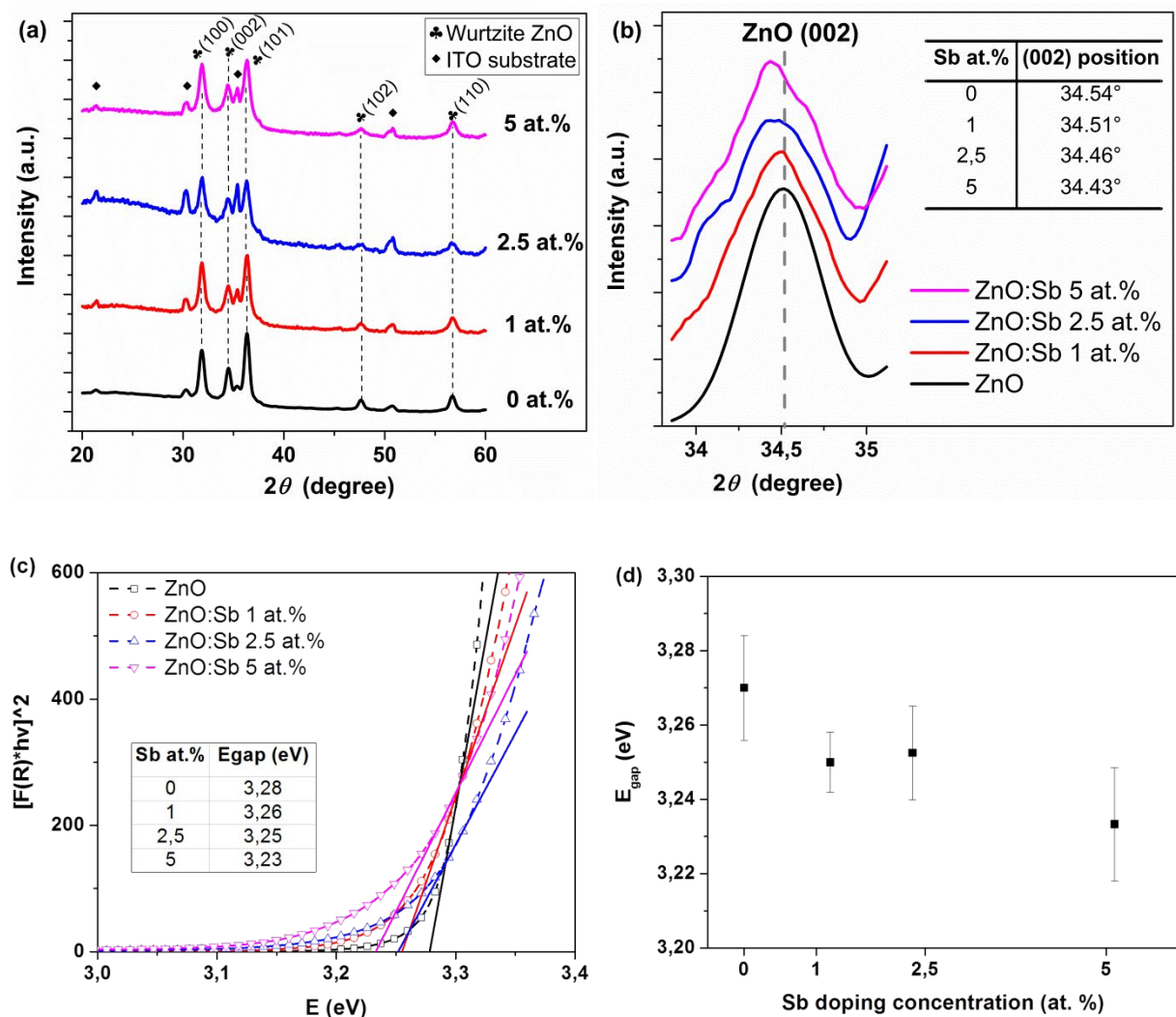
Figure 3. (a) XRD patterns for pristine ZnO and doped ZnO:Sb films. (b) Magnified view

of the (002) diffraction peak and shift of the corresponding 2θ position as a function of Sb

doping. (c) Tauc's plot for ZnO and ZnO:Sb porous films. (d) UV-Vis spectroscopy:

influence of Sb doping concentration on the Eg values.

The crystal structure of the investigated samples has been studied by X-Ray Diffraction (XRD). Figure 3a reports an overview of the diffractograms obtained for the pure and ZnO:Sb films. Generally, all of the samples crystallized in the hexagonal wurtzite structure, which is the most thermodynamically-stable phase for ZnO materials.[38] The main diffraction peaks are those positioned at 2θ angles of 31.8°, 34.5° and 36.2°, which belong to (100), (002) and (101) crystal planes, respectively. Other minor contributions at higher diffraction angles and typical of wurtzite ZnO have been detected as well. No additional peaks due to secondary Sb metallic or oxide phases are present, meaning that most of the Sb atoms are in the host ZnO lattice structure, and eventual Sb oxides are present in a few amount, i.e. below the XRD detection limit. Indeed, Sb doping strongly altered the crystallinity of the thin film. In particular, for the doped ZnO samples it is possible to highlight that the 2θ-position of the (002) diffraction plane is shifted towards lower angle values as compared to the pristine ZnO (see also the deconvolution of (002) peaks in Figure S1 of the Supporting Information, S.I.). In particular, Figure 3b evidences that the (002) peak became more broadened and shifted to lower 2θ angles by increasing the Sb at.%.[39] This stands for a stronger deformation of the ZnO crystalline framework

due to the higher amount of dopant introduced within the wurtzite lattice (5 at.%), with

bigger Sb atoms substituting at the Zn sites and thereby inducing a remarkable

deformation of the ZnO crystal unit cell, as also previously reported.[28, 39-41]

The optical properties have been investigated by means of UV-Vis spectroscopy and

the band-gap energy (E_g) is estimated according to the Tauc's method.[42] The introduction

of Sb dopant slightly changes the E_g value for the doped ZnO samples in comparison with

pristine ZnO one (Figure 3c,d). Despite this reduction being limited, it can be nevertheless

stated that the E_g value decreases by increasing the amount of Sb dopant, varying from

3.28 eV for pure ZnO to 3.23 eV for sample ZnO:Sb 5%. This change is expected to be

induced by the rise of additional shallow donors energy states in the ZnO band structure,

due to the introduction of Sb ions.[41]

Figure 4a,b shows IV curves and polarization curves obtained for the ZnO:Sb samples.

The remarkable current peaks present in the IV curves related to the sample ZnO:Sb 1

at.% at about ±200 V (black curve of panel a) are associated with the switching of the

ferroelectric domains.[27,28] Moreover, the corresponding polarization curves show

hysteresis loops and a non-zero residual polarization ranging between 2 μC cm^{-2} and 7.5

μC cm^{-2}, depending on the Sb doping level. In particular, it is found that sample ZnO:Sb

1 at.% exhibits good dielectric properties, with current values in the nA range outside of

the switching peaks region and the highest residual polarization value, thereby featuring

a quasi-ideal ferreoelectric behavior. On the other side, undesirable leakage currents in

the order of 10^{-6} A start to be present by further increasing the doping amount (samples

ZnO:Sb 2.5 at.% and ZnO:Sb 5 at.%). This leads to a loss of performances from a

dielectric point of view, causing a reduction of the residual polarization and a partial

suppression of the ferroelectric behavior. On the contrary, no ferroelectric phenomena

were found for the undoped ZnO sample, as shown by the absence of any switch current

peak and hysteresis loop in the corresponding IV and polarization curves of Figure S2 of

the Supporting Information (S.I.).
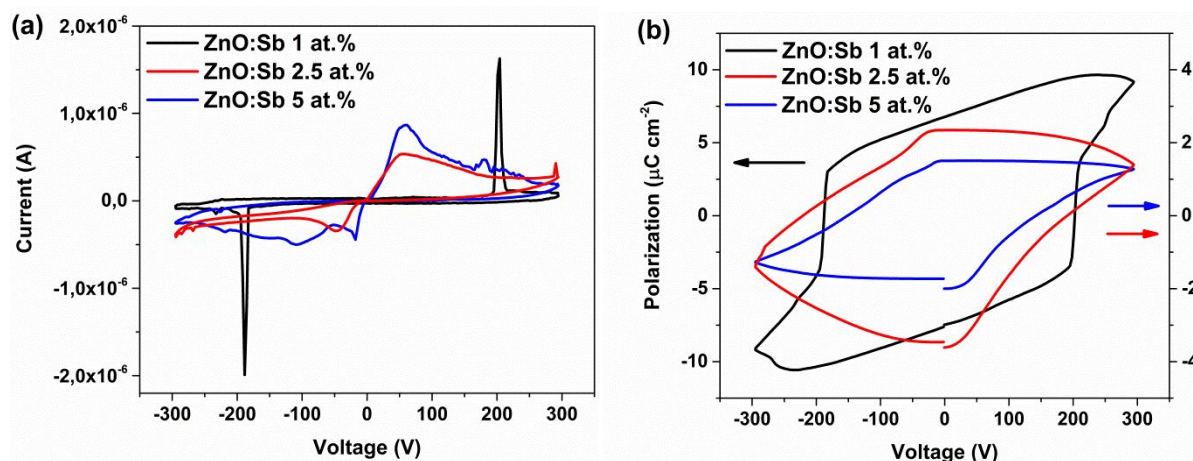
Figure 4. (a) I-V characteristic and (b) polarization curve for ZnO:Sb thin films.

The rise of ferroelectricity within ZnO:Sb thin films is due to the ionic radii difference between Zn and Sb ions that induces structural distortions, as well as variations in chemical bond strengths and polarities.[28] Both these factors induce the formation of permanent electric dipoles and the rise of the observed ferroelectric response. The loss of ferroelectricity for samples ZnO:Sb 2.5% and ZnO:Sb 5% is representative of their conducting behavior. This is most probably due to the higher amount of defects present in the corresponding crystalline structure,[43] which is significantly altered by the doping process as previously discussed (see also XRD patterns of Figure 3b).

From the results described so far, some key points can be preliminary highlighted in view of discussing the photo- and sonocatalytic behavior of the investigated materials. The first one deals with the morphological analysis. Independently of the presence of Sb dopant, a porous and high surface area has been noticed for all the samples.[28,33,37] This is a major requirement in designing new catalyst materials, as the presence of an extended surface area provides a larger number of active sites for dye adsorption and its

consequent degradation. It is also interesting to observe how the synthesis process for

preparing ZnO:Sb films did not change the morphology with respect to pristine ZnO one,

thereby preserving the surface area of the starting material. Secondly, the XRD analysis

pointed out a distortion of the ZnO crystal unit cell after the insertion of Sb dopant. This

deformation becomes more pronounced as long as the doping percentage is increased.

Such distortion of the crystal lattice has a twofold effect on the final material properties.

On the one hand, the reduced crystallinity is expected to introduce defects and additional

shallow donor states within the band gap structure of ZnO, thereby influencing the

corresponding optical properties.[41] In this regard, UV-Vis spectroscopic analyses pointed

out a reduction in the E_g value for ZnO:Sb thin films with respect to pristine ZnO, improving

the UV absorption properties of the ZnO:Sb catalyst. On the other hand, a high amount

of crystal defects can affect the charge transport properties of the material and influence

the corresponding photocatalytic behavior as well. Actually, those defects can act as

recombination centers for the photogenerated charge carriers, which should not

recombine together before reaching the outermost catalyst surface where the reactions

with the adsorbed dye molecules lead to its breakage and degradation. Another important

factor relates to the piezoelectric and ferroelectric behavior. Doping of ZnO with Sb has

been demonstrated a successful method to improve its piezoelectric response, but also

to confer ZnO new physical properties.[28] ZnO is a piezoelectric semiconductor with an

intrinsic n-type behavior associated with native surface/bulk defects and states. Such

native defects participate as free carriers and result in a mobile-charge-induced

polarization that partially suppresses the bound-charge-induced piezoelectric polarization

of the material. This effect is called "screening effect" and limits the piezoelectric response

of pure ZnO. The insertion of Sb element within the ZnO wurtzite structure allows to

partially compensate the intrinsic n-type behavior of ZnO and the resulting screening

effect. Actually, Sb doping of ZnO induces distortions and variations in the crystalline and

chemical structure and the rise of ferroelectric phenomena, as already previously reported

by some of us[28] and as represented in Figure 4. All the above-mentioned effects actively

participate in the reduction of the screening effect and improve the piezoelectric response.

Therefore, Sb doping is expected to influence the catalytic activity of the piezocatalysts

considered in this work as well.

2.2. Photocatalytic degradation of Rhodamine-β

The photocatalytic properties of ZnO and ZnO:Sb films have been studied by

considering the degradation of Rh-β organic dye under UV light irradiation, as shown in

Figure 5a. Without any catalyst (only the bare glass support is present), the sole effect of

UV light is almost negligible, with only 16% of Rh-β degradation achieved after 1 h, i.e.

the maximum irradiation time (see the black curve in Figure 5a and Figure S3 of the S.I.).

For the same time of irradiation, a degradation efficiency higher than 80% has been

obtained in presence of the catalyst and independently of the specific sample, i.e. pristine

ZnO rather than ZnO:Sb, thereby confirming the promising photocatalytic behavior of the

considered ZnO-based thin films. A positive influence of Sb doping level on the

photodegradation activity can be then highlighted if comparing the degradation

performances of the catalyst samples. Actually, the photodegradation properties of the

ZnO:Sb samples are superior, and further improve as long as the amount of Sb dopant

is increased. In particular, the best degradation efficiency (96% in 1 h) is obtained for the

most doped ZnO sample (ZnO:Sb 5 at.%). The degradation profiles of the photocatalytic

tests obey to a pseudo-first order kinetic law, as it can be observed from the fitting curves

reported in Figure 5b, also showing a good linear relationship ($R^2 > 0.981$) between the ln(C_0/C) and the time of irradiation. The slope of the straight line represents the kinetic constant (min^{-1}). Only the control test (without catalyst and only UV irradiation) reported a lower R^2 but those results were also reported for comparison purposes. Table 1 summarizes the main parameters describing the kinetic of degradation: kinetic constant and time necessary to degrade 50% of the initial amount of Rh-β ($t_{1/2}$). The highly doped ZnO sample (ZnO:Sb 5 at.%) displays the highest kinetic constant (0.048 min^{-1}) and lowest $t_{1/2}$ (14 min), in agreement with data reported in Figure 5a and showing that Rh-β degradation is almost complete at the end of the photodegradation experiment of 1 h.
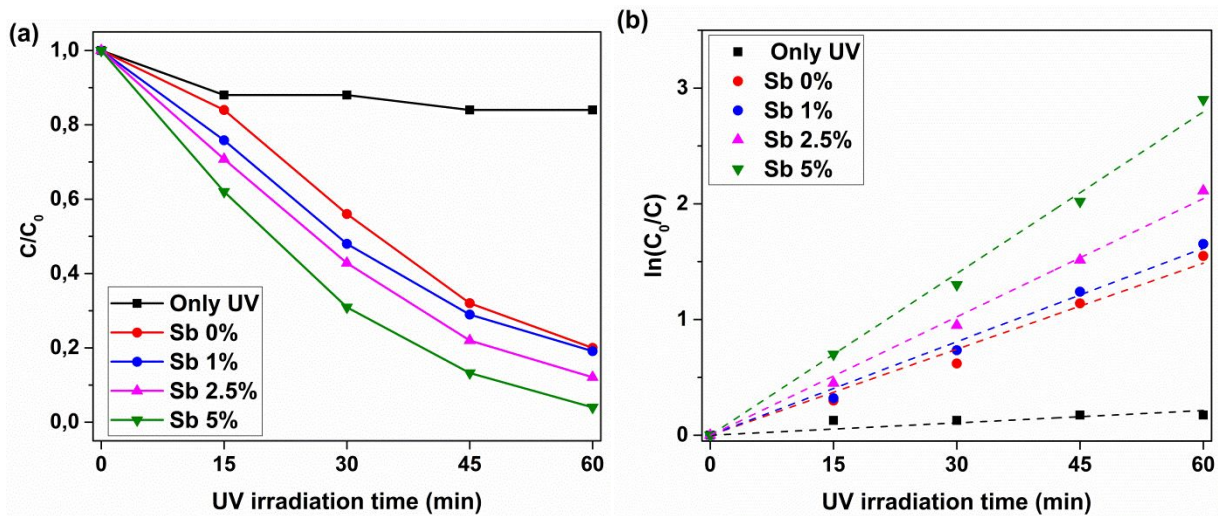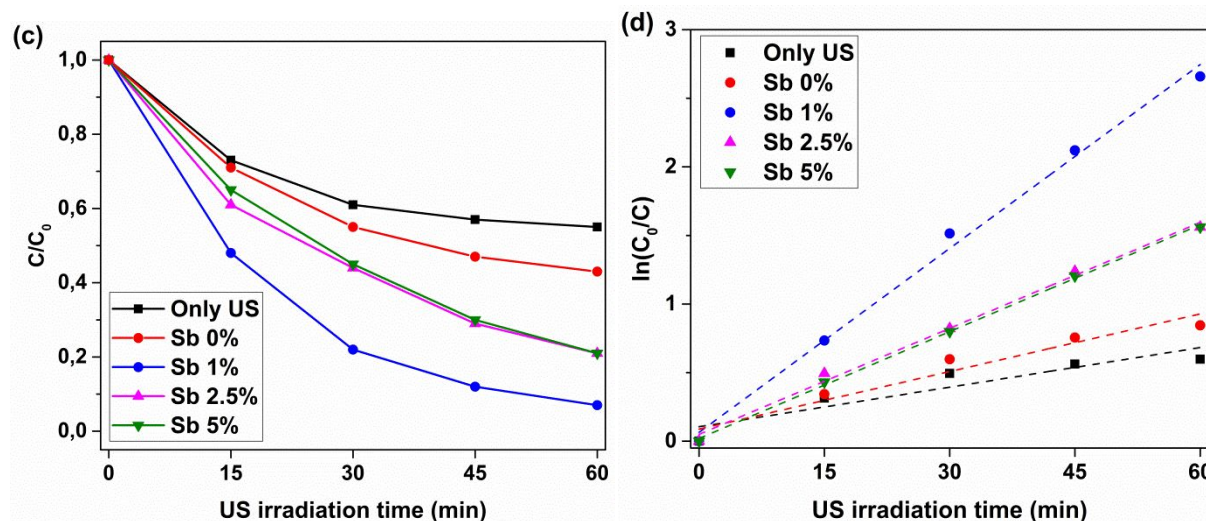
Figure 5. Photocatalytic (a, b) and piezocatalytic (c, d) degradation profiles of Rh-β dye

for the differently doped ZnO catalysts, as a function of the irradiation time. Fitting curves

are represented by dashed lines. Control experiments have been carried out on bare

ITO/glass substrates, i.e. without the ZnO-based catalysts.

The photodegradation results may be explained by considering the semiconducting

nature of ZnO and the optical properties of the investigated samples discussed

previously. As shown in Figures 3c and 3d, the band-gap energy value (Eg) is changed

after incorporating the Sb dopant, with a maximum Eg reduction achieved for the highest

doping level (5 at.%). The mechanism driving Rh-β photodegradation using

semiconductor catalysts is based on the photogeneration of free electrons due to light

absorption. The generated free carriers are then able to react with dye molecules

adsorbed on the outermost catalyst surface and with water molecules present in the

medium at the same time. In the first situation, the degradation of the dye is a direct

process and leads to the cleavage of xanthene chemical group (as discussed in the

following), dye decoloration and degradation. In the second case, the reaction between

the catalyst and the organic dye is mediated by highly reactive oxygen species (ROS)

generated from the interaction of free electrons with the hydroxyl groups present in the

chemical environment of the dye solution; ROS can easily attack the dye molecule and

induce its degradation.

For the same UV irradiation conditions, the observed decrease in the Eg value for

ZnO:Sb samples can further favor the photon absorption capability with respect to the

pure ZnO catalyst. Consequently, a higher number of electrons from the lower valence

band states of ZnO is promoted to the upper conduction band ones, leading to a superior

quantity of photogenerated carriers responsible for the dye degradation. The UV-induced

conduction electrons interact with OH- groups present in the water-based solution and

generate •OH radicals, as demonstrated in the following. The •OH species react with Rh-β

molecule, leading to the cleavage of Rh-β chemical groups and to the degradation of the

dye itself. It is well known that Rh-β in aqueous solutions has positively charged

diethylamino group -C=N$^+$(C$_2$H$_5$)$_2$ and at pH > 4 it is in the zwitterionic form due to the

dissociation of the carboxylic group (-COOH → -COO$^-$). Hence, two possible mechanisms

have been identified for Rh-β degradation, summarized in: (i) de-ethylation, a stepwise

process involving the dye adsorbed at a negatively charged catalyst surface, and (ii) the

cleavage of chromophore xanthene group due to the adsorption of the dye through the -

COO$^-$ at a positively charged catalyst surface.[21,44] The de-ethylation process is

responsible for the shift of the characteristic UV absorption peak of Rh-β, while the second

one deals with the cleavage of the cromophore group responsible for the dye color. This

cleavage is responsible for dye decoloration, which is represented by a strong reduction

of the UV peak intensity. In this work, no shift of the UV peak position has been observed,

while the reduction of the absorption peak intensity has been detected for all the

investigated samples (Figure S4 of the S.I.). Therefore, it may be concluded that the

dominant mechanism in all the degradation tests is the cleavage of the xanthene group.

This conclusion is further corroborated if considering that the surface charge of metal oxides and of the dye molecules are both pH-dependent.[45] ZnO-based materials generally exhibit an isoelectric point (IEP) at basic pH.[21,46,47] Therefore, at the operating pH conditions (5.8) the surface of the ZnO-based catalyst is expected to be positively-charged, thereby further promoting the adsorption of Rh-β (which is in zwitterionic form) through the -COO⁻ at the positively charged catalyst surface, and its degradation through the cleavage of chromophore xanthene group. A scheme summarizing the mechanisms leading to dye photodegradation is proposed in Figure 6.
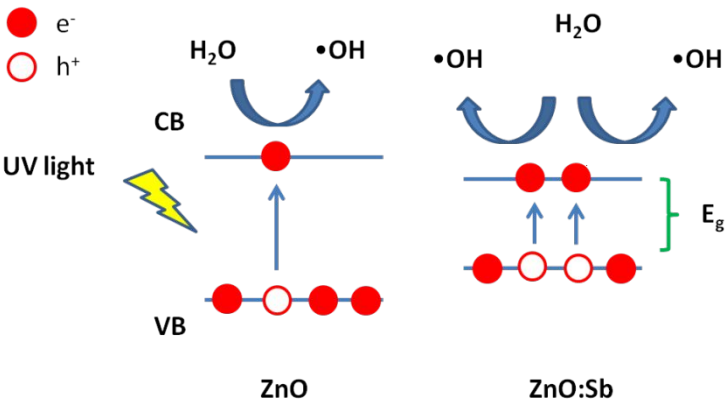
Figure 6. Mechanism of Rhodamine photodegradation using ZnO:Sb catalyst.

2.3. Piezocatalytic degradation of Rhodamine-β

The piezocatalytic experiments have been performed by irradiating the catalyst with US

waves and it is found that the presence of Sb dopant played a key role also in this case.

A continuous reduction in intensity of the Rh-β absorption peak has been observed

(Figure S5 of the S.I.) and the degradation of the dye approached 100% after 1 h of

irradiation in the best case, as it can be seen from Figure 5c. Similar to photodegradation,

Figure 5d and the good linear relationship between $\ln(C_0/C)$ and the time of US irradiation

represent that the degradation profiles follow a pseudo-first order kinetic law. As reported

in Table 1, the lowest efficiency has been obtained for pristine ZnO (57% degradation

after 1 h). By considering the doped samples, the most promising piezocatalytic behavior

has been shown by sample ZnO:Sb 1 at.% (93% efficiency), which has the highest kinetic

constant (0.045 min^{-1}) and the lowest $t_{1/2}$ (14 min). A good degradation behavior is

observed between samples ZnO:Sb 2.5 at.% and ZnO:Sb 5 at.%, with no significant

differences among them. The different behavior observed among the lowest and highest

doped ZnO samples can be inferred to the corresponding ferroelectric properties (Figure

4), as previously discussed. First of all, the investigated ZnO-based catalysts show

intrinsic piezoelectric properties.[28,34] Upon interaction with a mechanical stimulus (US

waves in this work), surface charge accumulation at the opposite sides of wurtzite

nanocrystals and the rise of an inner piezopotential can take place, favoring the

adsorption of charged dye molecules on the catalyst surface. Moreover, the presence of

an US-induced piezoelectric potential within the catalyst allows the generation of free

carriers able to react with the dye, then breaking the cromophore groups and leading to

dye degradation, similarly to what stated for photocatalysis. Both these effects are highly

enhanced if a permanent polarization within the catalyst is present, as for the doped

ZnO:Sb catalysts with 1 at.% content of Sb. Therefore, the overall effect is a superior

adsorption of charged species (dye molecules and hydroxyl groups) and a reduction in

recombination of free carriers generated by US irradiation, which result into the observed

improvement of the piezocatalytic properties of ZnO:Sb films with respect to the undoped,

non-ferroelectric ZnO counterpart.

2.4. Generation of reactive oxygen species under UV light/US irradiation

Electron Paramagnetic Resonance (EPR) spectroscopy coupled with the spin trapping

technique has been performed to investigate the ability of pure ZnO and ZnO:Sb samples

in generating reactive oxygen species (ROS) in water suspension, under both UV light

and US wave irradiation. Figure 7a reports the EPR spectra collected for the most

promising catalyst samples, i.e. pure ZnO and ZnO:Sb 5 at.%, in case of UV light

irradiation. With respect to the control sample (water + ITO-coated glass support), •OH

radicals are mostly generated in presence of the catalyst (ZnO and ZnO:Sb 5 at.%). In

particular, the amount of DMPO-OH spin adducts is slightly higher for the doped samples

(see Figure 7c) and confirms the superior photocatalytic properties of sample ZnO:Sb 5

at.% discussed previously. This favored generation of hydroxyl radicals is ascribable to

the lower band-gap energy. This further promotes photon absorption and the consequent

photogeneration of free e^-/h^+ carriers with respect to pure ZnO, which can react with OH^-

groups present in the water suspension and generate the corresponding radical species.
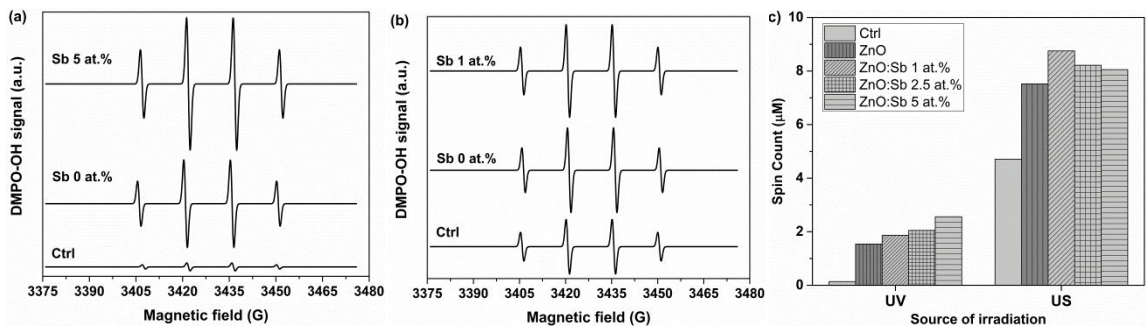
Figure 7. (a) EPR spectra for ZnO and ZnO:Sb 5% under UV light. (b) EPR spectra for ZnO and ZnO:Sb 1% films under US waves. (c) Quantitative estimation of DMPO-OH spin adduct generation from ZnO and ZnO:Sb films, under UV light and US irradiation. Control experiments have been carried out on bare ITO/glass substrates, i.e. without the ZnO-based catalysts.

Table 1. Kinetic parameters calculated from the kinetic plot and describing the photo- and piezocatalytic degradation process of ZnO and ZnO:Sb films.

Sample	$\%_{eff,\ max}$ [a]	Kinetic constant (K), [min^{-1}]	$t_{1/2,}$ [b] [min]	R-squared (R^2)
Only UV	16%	0.004	> 60	0.917
ZnO	80%	0.025	28	0.981
ZnO:Sb 1 at.%	81%	0.027	26	0.995
ZnO:Sb 2.5 at.%	88%	0.033	20	0.992
ZnO:Sb 5 at.%	96%	0.048	14	0.984
Only US	45%	0.009	> 60	0.889
ZnO	57%	0.014	43	0.956
ZnO:Sb 1 at.%	93%	0.045	14	0.994
ZnO:Sb 2.5 at.%	79%	0.026	25	0.994
ZnO:Sb 5 at.%	79%	0.026	25	0.999

[a] estimated at the end of the degradation experiment, i.e. after 60 minutes; [b] time after which 50% of the initial dye has been degraded.

When US is used as irradiation source, the difference in ROS generation between the control (glass/ITO substrate) and the catalysts (ZnO or ZnO:Sb-coated ITO/glass substrates) is not as remarkable as observed for UV light irradiation. As shown in Figure 7b, sonolysis of water due to US exposition is highly pronounced and a strong generation of •OH radicals is detected, even in absence of the catalyst. This is noticeable also from the color decay rate of Rh-β solution observed in absence on any ZnO-based catalyst, by merely applying US (control experiment, see Figures 5c and 5d). It can be also stated that hydroxyl radicals are more efficiently generated by applying US irradiation than UV light, as clearly depicted in Figure 7c. Anyway, the amount of ROS is higher in presence of the catalysts, especially in the case of Sb-doped ones. Similarly, to photocatalysis, the ultrasonic degradation of the dye can be associated to the generation of ROS also for piezocatalysis. However, the mechanism is different and two main contributions participating in dye degradation can be supposed to exist during US irradiation. ZnO is a piezoelectric material and it is also able to exhibit ferroelectric properties when doped with proper elements like Sb. In this work, the degradation rate between the pure and doped

samples during US irradiation is different, with the best performances exhibited from the

sample ZnO:Sb 1 at.%. The interaction of ZnO and ZnO:Sb films with US is expected to

induce the rise of a piezoelectric potential able to provide sufficient energy for separating

electron-hole pairs. The so-generated free carriers are thus able to interact with water

present in the dye solution, producing ROS and provoking the degradation of the dye.

However, when ferroelectric ZnO:Sb samples are considered, an additional effect can be

accounted and is related to the existence of a permanent ferroelectric polarization.

Actually, as shown in Figure 4, an inner electric field, additional to piezopotential, is able

to improve the adsorption of charged species from the chemical environment (dye

molecules and hydroxyl groups). Moreover, this inner field also reduces the

recombination rate of free carriers that generally limit the performances of semiconductor

catalysts like ZnO. The synergy of the abovementioned contributions allows a more

efficient reaction between OH^- groups and free carriers, enhancing the production of •OH

radicals with respect to pure ZnO (see Figure 7c) and finally improving the degradation

efficiency of the overall system.

3. Conclusion

Piezoelectric ZnO and ZnO:Sb thin films have been prepared by a simple approach based on RF magnetron sputtering, a wet impregnation of the sputtered layers into the doping solution and a final thermal treatment. The physical-chemical characterization results confirmed the correct insertion of the Sb dopant in the host ZnO crystalline lattice. With respect to the undoped ZnO counterpart, the ZnO:Sb samples showed a reduction in the band-gap energy as a function of the doping percentage, as also the rise of ferroelectricity represented by well-defined switch current peaks along with a permanent electrical polarization. The photo- and piezocatalytic properties of the considered materials have been evaluated by studying the degradation of Rh-β dye under UV light and US waves irradiation. Independently of the irradiation source, the ZnO:Sb catalysts showed superior properties with respect to pure ZnO, with a kinetic constant being 5-12 fold higher in the best scenario. The mechanism leading to dye degradation also involves the generation of ROS, which has been validated by EPR spectroscopy, both under UV light and US waves irradiation. The best photocatalytic behavior has been observed for the maximum Sb doping percentage (5 at.%), which allowed a sufficient reduction of the

band-gap energy and improved the corresponding photogeneration of free electrons and catalytic properties. On the other side, the most promising piezocatalytic efficiency was obtained by using the minimum amount of Sb dopant (1 at.%), which actually exhibited the best ferroelectric behavior. In this case, the presence of a permanent electrical polarization within the doped catalyst, coupled with the presence of a piezopotential, allowed the generation of free carriers and the reduction of charge recombination phenomena. This permanent polarization also helped in recalling charged species from the dye solution, i.e. Rh-β^+ and OH$^-$, further favoring their absorption on the catalyst surface.

4. Experimental Section

Synthesis of pristine ZnO and ZnO:Sb thin films: commercial Indium Tin Oxide (ITO)-coated soda lime glass slides (12 Ω sq^{-1}, VisionTek Systems Ltd.) were used as substrates. The ITO/glass supports were cleaned with acetone and ethanol in ultrasound bath for 10 min, then finally dried under nitrogen flow.

Porous Zn films were deposited on the cleaned ITO-glass substrates by RF magnetron

sputtering at room temperature for 2 h.[34] The substrates were placed on the substrate

holder facing upwards to the target, with a target-to-substrate distance of around 8 cm.

Before starting the deposition, suitable high-vacuum conditions (base pressure around

9×10^{-8} Torr) were created within the deposition chamber by a two-stage pumping system

consisting of a rotary and turbomolecular pumps. Then, pure Ar (10 sccm flow, 5×10^{-3}

Torr pressure) was injected into the sputtering deposition chamber. A RF signal voltage

(13.56 MHz operating frequency, RF power value of 30 Watt) was applied to the cathode

on which the source material is clamped, and used to create plasma. A 4-inch diameter

pure Zn target was used as source material and the substrate temperature was monitored

by a thermocouple during the whole deposition process. A pre-sputtering of the target

was performed for 10 min in pure Ar atmosphere to remove any contaminant from the

source material. The final average thickness of the prepared samples was around 3.5

µm.

Antimony dopant (Sb) was introduced by wet-impregnation of the porous metallic Zn

layers in Sb precursor solution,[28] prepared by dissolving antimony acetate ($C_6H_9O_6Sb$,

Sigma-Aldrich, 99.98% purity, 0.12 mg mL^{-1}) in bidistilled water (final volume of 50 mL).

The porous Zn films were soaked in the doping solution under continuous stirring at 50

°C for different times (1 h, 3 h and 6 h). After, the impregnated samples were thermally

treated in a muffle furnace operating in air, at 380 °C, for 2 h (heating rate 150 °C h^{-1}).

Impregnation times lower than 1 h (i.e. 30 min) did not lead to any significant doping of

the final material, while dissolution of the Zn film was observed for higher impregnation

times (i.e., 8 h, 16 h).

As a reference, pristine ZnO films were prepared according to a similar experimental

procedure, avoiding the impregnation of the samples in the doping solution. At the end of

the synthesis process, each sample was properly weighed and an average amount of 3

mg of material has been estimated.

UV light and US wave-aided degradation experiments. Rhodamine-β (Rh-β) powder (1

mg) was dissolved in bi-distilled water (final volume of 400 mL, concentration of 2.5 ppm,

pH=5.8), under continuous stirring at room temperature and in dark conditions. A

calibration curve was obtained by considering the characteristic UV absorbance value of

Rh-β at λ=554 nm, obtained for different solutions prepared at prefixed concentration

values (Figure S6 of the S.I.). The amount of catalyst employed for each degradation experiment has been estimated in 3 mg, as mentioned previously, in 10 mL of dye solution. All the control experiments have been carried in presence of a bare ITO-coated glass support.

Photodegradation experiments were performed by using a UV lamp (High Power Mercury-Xenon Light Source, Newport, 500 W, Wavelength 350–450 nm). The Rh-β solution (10 mL) was maintained homogeneous by continuous stirring at 360 rpm. The catalyst sample was placed atop of a Teflon® support within a cylindrical Pyrex reactor and soaked at room temperature in the Rh-β solution. Before irradiation, the catalyst sample was left in contact with the dye solution in dark conditions and under continuous stirring for 20 min, in order to achieve adsorption-desorption equilibrium conditions between dye and the catalyst (dark phase). Then, light irradiation was performed from the upper side of the solution. The distance between the solution and the source was fixed at 8 cm to ensure 150 mW cm^{-2} of UV light irradiation intensity.

Piezodegradation experiments were performed by using a commercial US transducer apparatus (Lipozero).[48] The catalyst sample was placed within a 6-well microplate and

the single well filled with Rh-β solution (10 mL). Then, US irradiation was performed from the bottom. A water-based gel was placed between the microplate and the transducer in order to maximize the coupling between the propagating US and the sample. The US parameters for piezodegradation experiments were as follows: signal frequency, 1 MHz; US power, 1.2 W cm^{-2}; duty cycle, 100%. Similar to photodegradation experiments, dark phase was achieved before US irradiation by leaving the catalyst in contact with Rh-β solution in dark conditions for 20 min.

The color decay of Rh-β solution under both UV and US irradiation was investigated by means of UV absorbance spectroscopy. 100 μL was withdrawn from the dye solution at regular points of time (15 min, 30 min, 45 min, 60 min) and the corresponding UV absorbance spectrum acquired with a microplate reader (Multiskan go, ThermoScientific). From the recorded UV absorption spectra (Figures S4 and S5) and according to the calibration curve (Figure S6), the efficiency of dye degradation has been estimated as C/C_0 (%), where C represents the concentration of solution at time t and C_0 is the initial one. UV- and US-driven dye degradation processes have been evaluated according to the following pseudo first-order kinetic equation:

$$ln\left(\frac{C_0}{C}\right) = kt$$

with k representing the kinetic rate constant and defined as:

$$k = \frac{ln\left(\frac{C_0}{C}\right)}{t}$$

Characterization setup. The morphology of the samples was investigated using a Carl-Zeiss dual-beam Auriga field emission scanning electron microscope (FESEM) coupled with an Oxford Instruments X-Max 50 mm^2 silicon drift detector (SDD) for EDX analyses. The crystal structure and orientation was investigated by XRD measurements using a Panalytical X'Pert X-ray diffractometer in the Bragg–Brentano configuration (Cu Kα radiation, λ = 1.54059 Å). The optical properties have been evaluated by UV-Vis spectra, collected with a Cary 5000 Scan UV–vis spectrophotometer using a total reflectance sphere. All the spectra were background subtracted. The energy band-gap was estimated according to Tauc's plot. The electrical properties were evaluated by using a Piezo Evaluation System (PES, TFAnalyzer 2000HS, Aixacct). Measurements were performed

under the application of a triangular excitation signal (voltage amplitude 300 V, frequency

0.5 Hz). The evaluation of hydroxyl radical species generation was carried out by means

of the EPR-spin trapping technique coupled with the spin trap 5,5-dimethyl-L-pyrroline-N-

oxide (DMPO, 10 M) (Sigma, St. Louis, MO, USA). The detection of UV- and US-induced

radical species was obtained by adding 1 mL of the selected spin trap (final concentration

10 mM) to 9 mL of deionized water (total volume of the sample, 10 mL), in presence of

the ZnO-based catalyst. Bare ITO-coated glass supports have been used for control

experiments. In each case, the solution was irradiated with UV light (Wavelength 350–

450 nm, Intensity: 150 mW cm^{-2}) or with US for 30 min and then promptly collected with

a quartz microcapillary tube. The microcapillary tubes were then transferred into the EPR

cavity and the spectra were recorded by using a Bruker EMXnano X-Band spectrometer

(Bruker, Billerica, MA, USA). The EPR measurement parameters were as follows:

frequency, 9.74 GHz; scan width, 100 G; receiver gain, 60 dB; sweep time, 60 s; n. of

scans, 10. After acquisition, the spectrum was processed using the Bruker Xenon

software (Bruker, Billerica, MA, USA) for baseline correction and spin count.

ASSOCIATED CONTENT

Supporting Information

Deconvolution of (002) diffraction peak for pure ZnO and ZnO:Sb films. I-V

characteristic and polarization curve for undoped ZnO thin film. UV-Vis absorption

spectra of Rh-β solution under UV/Us irradiation without the presence of the catalyst.

UV-Vis absorption spectra of Rh-β solution obtained after photodegradation by UV light

and piezodegradation by US waves stimulation, in presence of pure ZnO and Sb-doped

ZnO catalysts. UV absorption spectra and calibration curve for Rh-β aqueous solutions

prepared at prefixed concentrations. EPR spectra for ZnO and ZnO:Sb thin films under

UV light and US waves irradiation.

AUTHOR INFORMATION

Corresponding Author

* E-mail: valentina.cauda@polito.it

ABBREVIATIONS

UV, ultraviolet; US, ultrasound; Rh-β, Rhodamine B; AOPs; advanced oxidation processes; ROS, reactive oxygen species; BT, barium titanate; ZnO, zinc oxide; GRAS, generally-recognized-as-safe; MB, methylene blue; FESEM, field emission scanning electron microscopy; EDS, energy dispersive X-ray spectroscopy; XRD, X-Ray Diffraction; IEP, isoelectric point; EPR, Electron Paramagnetic Resonance spectroscopy; DMPO, 5,5-dimethyl-L-pyrroline-N-oxide.

REFERENCES

(1)   Boretti, A.; Rosa, L. Reassessing the Projections of the World Water Development Report. *Npj Clean Water* **2019**, *2*.

(2)   Behrens, H.; Beims, U.; Dieter, H.; Dietze, G.; Eikmann, T.; Grummt, T.; Hanisch, H.; Henseling, H.; Käß, W.; Kerndorff, H.; Leibundgut, C.; Müller-Wegener, U.; Rönnefahrt, I.; Scharenberg, B.; Schleyer, R.; Schloz, W.; Tilkes, F., Toxicological and ecotoxicological assessment of water tracers. Hydrogeology Journal 2001, 9 (3), 321-325.

(3)   Crini, G.; Lichtfouse, E. Advantages and Disadvantages of Techniques Used for Wastewater Treatment. *Env. Chem. Lett.* **2019**, *17*, 145.

(4)   Xu, C. P.; Anusuyadevi, P. R.; Aymonier, C.; Luque, R.; Marre, S. Nanostructured Materials for Photocatalysis. *Chem. Soc.y Rev.* **2019**, *48*, 3868.

(5)   Starr, M. B.; Shi, J.; Wang, X. D. Piezopotential-Driven Redox Reactions at the Surface of Piezoelectric Materials. *Angew. Chem.-Int. Ed.* **2012**, *51*, 5962.

(6)   Liang, Z.; Yan, C. F.; Rtimi, S.; Bandara, J. Piezoelectric Materials for Catalytic/Photocatalytic Removal of Pollutants: Recent Advances and Outlook. *Appl. Catal. B-Env.* **2019**, *241*, 256.

(7)   Wu, J.; Qin, N.; Bao, D. H. Effective Enhancement of Piezocatalytic Activity of Batio$_3$ Nanowires under Ultrasonic Vibration. *Nano Energy* **2018**, *45*, 44.

(8)   Li, H. D.; Sang, Y. H.; Chang, S. J.; Huang X.; Zhang, Y.; Yang, R. S.; Jiang, H. D.; Liu, H.; Wang, Z. L. Enhanced Ferroelectric-Nanocrystal-Based Hybrid Photocatalysis by Ultrasonic-Wave-Generated Piezophototronic Effect. *Nano Lett.* **2015**, *15*, 2372.

(9)   Hong, K. S.; Xu, H. F.; Konishi, H.; Li, X. C. Direct Water Splitting Through Vibrating Piezoelectric Microfibers in Water. *J. Phys. Chem. Lett.* **2010**, *1*, 997.

(10)   Lv, W.; Kong, L. J.; Lan, S. Y.; Feng, J. X.; Xiong, Y.; Tian, S. H. Enhancement Effect in the Piezoelectric Degradation of Organic Pollutants by Piezo-Fenton Process. *J. Chem. Technol. Biot.* **2017**, *92*, 152.

(11)   Lin, H.; Wu, Z.; Jia, Y. M.; Li, W. J.; Zheng, R. K.; Luo, H. S. Piezoelectrically Induced Mechano-Catalytic Effect for Degradation of Dye Wastewater Through Vibrating Pb(Zr0.52Ti0.48)O-3 Fibers. *Appl. Phys. Lett.* **2014**, *104*, 162907.

(12)   Feng, Y. W.; Ling, L. L.; Wang, Y. X.; Xu, Z. M.; Cao, F. L.; Li, H. X.; Bian, Z. F. Engineering Spherical Lead Zirconate Titanate to Explore the Essence of Piezo-Catalysis. *Nano Energy* **2017**, *40*, 481.

(13)   Mushtaq, F.; Chen, X. Z.; Hoop, M.; Torlakcik, H.; Pellicer, E.; Sort, J.; Gattinoni, C.; Nelson, B. J.; Pane, S. Piezoelectrically Enhanced Photocatalysis with BiFeO$_3$ Nanostructures for Efficient Water Remediation. *Iscience* **2018**, *4*, 236.

(14)   Rodnyi, P. A.; Khodyuk, I. V. Optical and Luminescence Properties of Zinc Oxide. *Opt. Spectrosc.* **2011**, *111*, 776.

(15)   Kou, L. Z.; Guo, W. L.; Li, C. Piezoelectricity of ZnO and its Nanostructures. Proceedings of the 2008 Symposium on Piezoelectricity, Acoustic Waves and Device Applications **2008**, 354.

(16)   Laurenti, M.; Stassi, S.; Canavese, G.; Cauda, V. Surface Engineering of Nanostructured ZnO Surfaces. *Adv. Mater. Interfaces* **2017**, *4*, 1600758.

(17)   Dumontel, B.; Canta, M.; Engelke, H.; Chiodoni, A.; Racca, L.; Ancona, A.; Limongi, T.; Canavese, G.; Cauda, V. Enhanced Biostability and Cellular Uptake of Zinc Oxide Nanocrystals Shielded with a Phospholipid Bilayer. *J. Mater. Chem. B* **2017**, *5*, 8799.

(18)   Laurenti, M.; Cauda, V.; Gazia, R.; Fontana, M.; Rivera, V.F.; Bianco, S.; Canavese, G. Wettability Control on ZnO Nanowires Driven by Seed Layer Properties. *Eur. J. Inorg. Chem.* **2013**, *14*, 2520.

(19)   Laurenti, M.; Verna, A.; Fontana, M.; Quaglio, M.; Porro, S. Selective Growth of ZnO Nanowires on Substrates Patterned by Photolithography and Inkjet Printing. *Appl. Phys. A-Mater. Sci. Proc.* **2014**, *117*, 901.

(20)   Shen, W. Z.; Li, Z. J.; Wang, H.; Liu, Y. H.; Guo, Q. J.; Zhang, Y. L. Photocatalytic Degradation for Methylene Blue using Zinc Oxide Prepared by Codeposition and Sol-Gel Methods. *J. Hazard. Mater.* **2008**, *152*, 172.

(21)   Lops, C.; Ancona, A.; Di Cesare, K.; Dumontel, B.; Garino, N.; Canavese, G.; Hernandez, S.; Cauda, V. Sonophotocatalytic Degradation Mechanisms of Rhodamine B Dye via Radicals Generation by Micro- and Nano-Particles of ZnO. *Appl. Catal. B-Environ.l* **2019**, *243*, 629.

(22)   Kumar, R.; Kumar, G.; Umar, A. Zinc Oxide Nanomaterials for Photocatalytic Degradation of Methyl Orange: A Review. *Nanosci. Nanotech. Lett.* **2014**, *6*, 631.

(23)   Zhu, D.; Zhou, Q. Action and Mechanism of Semiconductor Photocatalysis on Degradation of Organic Pollutants in Water Treatment: a Review. *Env. Nanotech. Monit. Manag.* **2019**, 12, 100255.

(24)   Xue, X. Y.; Zang, W. L.; Deng, P.; Wang, Q.; Xing, L. L.; Zhang, Y.; Wang, Z. L. Piezo-Potential Enhanced Photocatalytic Degradation of Organic Dye using ZnO Nanowires. *Nano Energy* **2015**, *13*, 414.

(25)   Paganini, M. C.; Giorgini, A.; Goncalves, N. P. F.; Gionco, C.; Prevot, A. B.; Calza, P. New Insight into Zinc Oxide Doped with Iron and its Exploitation to Pollutants Abatement. *Catal. Today* **2019**, *328*, 230.

(26)   Ba-Abbad, M. M.; Kadhum, A. A. H.; Mohamad, A.; Takriff, M. S.; Sopian, K. Visible Light Photocatalytic Activity of Fe^{3+}-Doped ZnO Nanoparticle Prepared Via Sol-Gel Technique. *Chemosphere* **2013**, *91*, 1604.

(27)   Laurenti, M.; Castellino, M.; Perrone, D.; Asvarov, A.; Canavese, G.; Chiolerio, A. Lead-Free Piezoelectrics: V^{3+} to V^{5+} Ion Conversion Promoting the Performances of V-Doped Zinc Oxide. *Sci. Rep.* **2017**, *7*, 41957.

(28)   Laurenti, M.; Canavese, G.; Sacco, A.; Fontana, M.; Bejtka, K.; Castellino, M.; Pirri, C. F.; Cauda, V. Nanobranched ZnO Structure: p-Type Doping Induces Piezoelectric Voltage Generation and Ferroelectric-Photovoltaic Effect. *Adv. Mater.* **2015**, *27*, 4218.

(29)   Liu, C.; Yu, A.; Peng, M.; Song, M.; Liu, W.; Zhang, Y.; Zhai, J., Improvement in the Piezoelectric Performance of a ZnO Nanogenerator by a Combination of Chemical Doping and Interfacial Modification. *J. Phys. Chem. C* **2016**, *120* (13), 6971-6977.

(30)   Lee, K. M.; Lai, C. W.; Ngai, K. S.; Juan, J. C., Recent developments of zinc oxide based photocatalyst in water treatment technology: A review. *Water Res.* **2016**, *88*, 428-448.

(31)   Wu, J. M.; Hsu, G. K.; Yeh, H.-H.; Lin, H.-C., Metallic Zinc Nanowires Effect in High-Performance Photoresponsive and Photocatalytic Properties of Composite Zinc Stannate Nanowires. *J. Electrochem. Soc.* **2012,** *159* (5), H497-H501.

 (32)   Wang, Y.-C.; Wu, J. M., Effect of Controlled Oxygen Vacancy on H2-Production through the Piezocatalysis and Piezophototronics of Ferroelectric R3C ZnSnO3 Nanowires. *Adv. Funct. Mater.* **2020,** *30* (5), 1907619.

(33)   Gazia, R.; Chiodoni, A.; Bianco, S.; Lamberti, A.; Quaglio, M.; Sacco, A.; Tresso, E.; Mandracci, P.; Pirri, C. F. An Easy Method for the Room-Temperature Growth of Spongelike Nanostructured Zn Films as Initial Step for the Fabrication of Nanostructured ZnO. *Thin Solid Films* **2012**, *524*, 107.

(34)   Laurenti, M.; Canavese, G.; Stassi, S.; Fontana, M.; Castellino, M.; Pirri, C. F.; Cauda, V. A Porous Nanobranched Structure: an Effective Way to Improve Piezoelectricity in Sputtered ZnO Thin Films. *RSC Adv.* **2016**, *6*, 76996.

(35)   Thornton, J. A., High Rate Thick Film Growth. *Annu. Rev. Mater. Sci.,* **1977,** *7* (1), 239-260.

(36)   A. F. Jankowski, J. P. Hayes, Innovations in the vapor deposition of metal coatings for target payloads in laser-based physics experiments under extreme conditions. *J. Vac. Sci. Technol., A*, **2003**, *21*, 422–425.

(37)   Laurenti, M.; Cauda, V. Gentamicin-Releasing Mesoporous ZnO Structures. *Materials* **2018**, *11*(2), E314.

(38)   Ashrafi, A.; Jagadish, C. Review of Zincblende ZnO: Stability of Metastable ZnO Phases. *J. Appl.Phys.* **2007**, *102*, 071101.

(39)   Yang, Y.; Qi, J. J.; Liao, Q. L.; Zhang, Y.; Tang, L. D.; Qin, Z. Synthesis and Characterization of Sb-Doped ZnO Nanobelts with Single-Side Zigzag Boundaries. *J. Phys. Chem. C* **2008**, *112*, 17916.

(40)   Lupan, O.; Chow, L.; Ono, L. K.; Roldan Cuenya, B.; Chai, G. Y.; Khallaf, H.; Park, S.; Schulte, A. Synthesis and Characterization of Ag- or Sb-Doped ZnO Nanorods by a Facile Hydrothermal Route. *J. Phys. Chem. C* **2010**, *114*, 12401.

(41)   Samanta, K.; Bhattacharya, P.; Katiyar, R. S. Raman Scattering Studies of P-Type Sb-Doped ZnO Thin Films. *J. Appl. Phys.* **2010**, *108*, 113501.

(42)   Reddy, K. M.; Manorama, S. V.; Reddy, A. R. Bandgap Studies on Anatase Titanium Dioxide Nanoparticles. *Mater. Chem. Phys.* **2003**, *78*, 239.

(43)   Gazia, R.; Canavese, G.; Chiodoni, A.; Lamberti, A.; Stassi, S.; Sacco, A.; Bianco, S.; Virga, A.; Tresso, E.; Pirri, C. F. Novel Spongelike Nanostructured ZnO Films: Properties and Applications. *J. Alloy. Compd.* **2014**, *586*, S331.

(44)   Rasheed, T.; Bilal, M.; Iqbal, H. M. N.; Hu, H. B.; Zhang, X. H. Reaction Mechanism and Degradation Pathway of Rhodamine 6G by Photocatalytic Treatment. *Water Air Soil Poll*. **2017**, *228,* 291.

(45)   Shimizu, N.; Ogino, C.; Dadjour, M. F.; Murata, T., Sonocatalytic degradation of methylene blue with TiO2 pellets in water. *Ultrason Sonochem* **2007,** *14* (2), 184-190.

(46)   Ancona, A.; Dumontel, B.; Garino, N.; Demarco, B.; Chatzitheodoridou, D.; Fazzini, W.; Engelke, H.; Cauda, V., Lipid-Coated Zinc Oxide Nanoparticles as Innovative ROS-Generators for Photodynamic Therapy in Cancer Cells. *Nanomaterials* **2018,** *8* (3), 143.

(47)   Marsalek, R., Particle Size and Zeta Potential of ZnO. *APCBEE Procedia* **2014,** *9*, 13-17.

(48)   Vighetto, V.; Ancona, A.; Racca, L.; Limongi, T.; Troia, A.; Canavese, G.; Cauda, V. The Synergistic Effect of Nanocrystals Combined with Ultrasound in the Generation of Reactive Oxygen Species for Biomedical Applications. *Front. Bioeng. Biotech.* **2019**, *7*, 374.

ToC figure